Supporting Information (SI)

An Artificial Z-Scheme Constructed from Dye-Sensitized Metal Oxide Nanosheets for Visible Light-Driven Overall Water Splitting

Takayoshi Oshima,[a,b,$] Shunta Nishioka,[a,b,c] Yuka Kikuchi,[d] Shota Hirai,[a] Kei-ichi Yanagisawa,[e] Miharu Eguchi,[f] Yugo Miseki,[g] Toshiyuki Yokoi,[h] Tatsuto Yui,[d] Koji Kimoto,[e] Kazuhiro Sayama,[g] Osamu Ishitani,[a] Thomas E. Mallouk,[c,i] Kazuhiko Maeda*[a]*

[a] Department of Chemistry, School of Science, Tokyo Institute of Technology, 2-12-1-NE-2 Ookayama, Meguro-ku, Tokyo 152-8550, Japan

[b] Japan Society for the Promotion of Science, Kojimachi Business Center Building, 5-3-1 Kojimachi, Chiyoda-ku, Tokyo 102-0083, Japan

[c] Department of Chemistry, University of Pennsylvania, 231 S. 34th Street, Philadelphia, PA 19104-6363, United States

[d] Graduate School of Science and Technology, Niigata University, 8050 Ikarashi-2, Niigata 950−2181, Japan

[e] Research Center for Advanced Measurement and Characterization, National Institute for Materials Science (NIMS), 1-1 Namiki, Tsukuba, Ibaraki 305-0044, Japan

[f] Research Center for Functional Materials, National Institute for Materials Science (NIMS), 1-1 Namiki, Tsukuba, Ibaraki 305-0044, Japan

[g] Research Center for Photovoltaics (RCPV) and Global Zero Emission Research Center (GZR), National Institute of Advanced Industrial Science and Technology (AIST), Central 5, 1-1-1 Higashi, Tsukuba, Ibaraki, 305-8565 Japan

[h] Nanospace Catalysis Unit, Institute of Innovative Research, Tokyo Institute of Technology, 4259-S2-5, Nagatsuta, Midori-ku, Yokohama 226-8503, Japan

[i] International Center for Materials Nanoarchitectonics (WPI-MANA), National Institute for Materials Science (NIMS), 1-1 Namiki, Tsukuba, Ibaraki 305-0044, Japan

[$] Max Planck Institute for Solid State Research, Heisenbergstr. 1, Stuttgart 70569, Germany

*To whom corresponding authors should be addressed.

T.E.M.: mallouk@sas.upenn.edu; K.M.: maedak@chem.titech.ac.jp

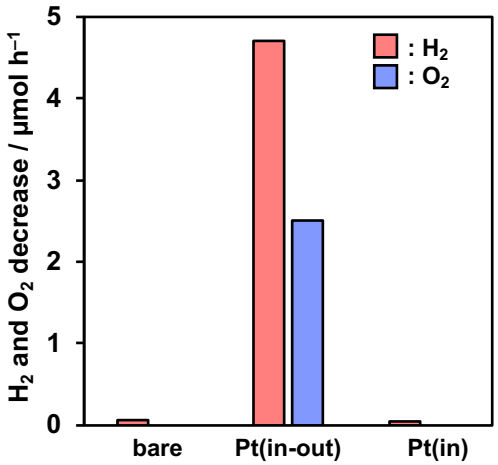

Figure S1. Rates of H_2 and O_2 decrease on bare $HCa_2Nb_3O_{10}$, Pt(in-out)/$HCa_2Nb_3O_{10}$ and Pt(in)/$HCa_2Nb_3O_{10}$. Reaction conditions: catalyst, 20 mg; solution, pure water (100 mL); initial amount of H_2 and O_2: ca. 200 and 100 μmol, respectively. The reaction proceeds efficiently on Pt particles deposited on the external surface, whereas intercalated Pt does not contribute to the reaction because H_2 and O_2 do not have access to the interlayer space.[S1] Actually, H_2 and O_2 were consumed at measurable rates on the Pt(in-out)/$HCa_2Nb_3O_{10}$, whereas no reaction took place on Pt(in)/$HCa_2Nb_3O_{10}$. These results indicate that Pt species deposited on the external surface of the $HCa_2Nb_3O_{10}$ nanosheet samples were completely removed by the aqua regia treatment.

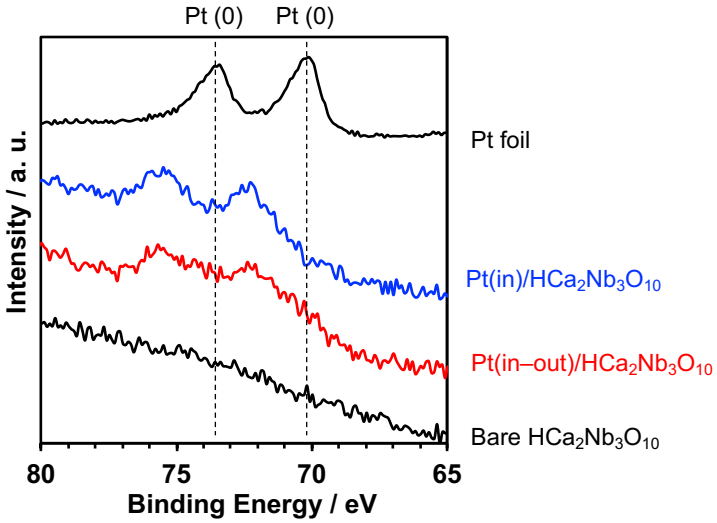

Figure S2. Pt-4f XPS spectra of bare $HCa_2Nb_3O_{10}$, Pt(in-out)/$HCa_2Nb_3O_{10}$ and Pt(in)/$HCa_2Nb_3O_{10}$ nanosheets. A spectrum of Pt foil was also shown as a reference.

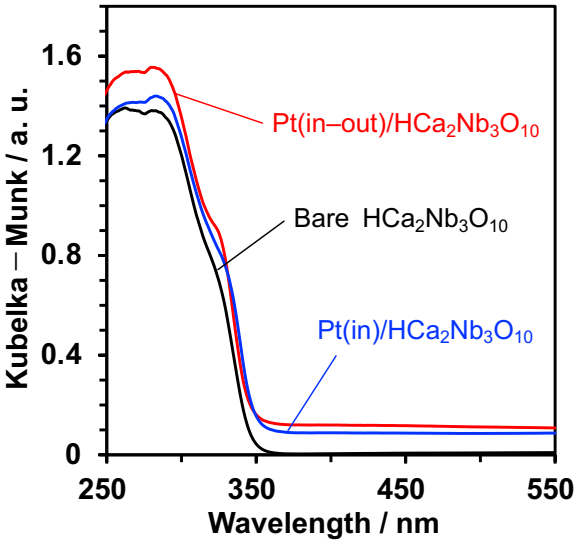

Figure S3. UV-visible DRS of bare $HCa_2Nb_3O_{10}$, Pt(in-out)/$HCa_2Nb_3O_{10}$ and Pt(in)/$HCa_2Nb_3O_{10}$ nanosheets. The increase in the absorption background in the longer wavelength region indicates the presence of Pt species on $HCa_2Nb_3O_{10}$ nanosheets even after the aqua regia treatment.

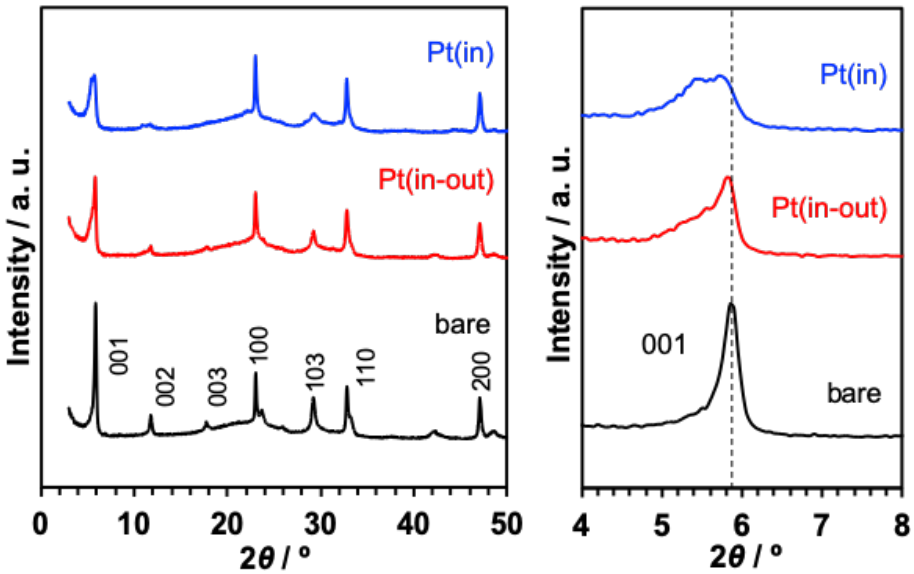

Figure S4. XRD patterns of bare $HCa_2Nb_3O_{10}$, Pt(in-out)/$HCa_2Nb_3O_{10}$ and Pt(in)/$HCa_2Nb_3O_{10}$ nanosheets. The diffraction peak attributed to the (001) reflection, which is the layer stacking direction, was shifted to lower two-theta angle, with a new shoulder peak upon Pt deposition, demonstrating an expansion of the (001) interlayer distance due to an intercalation of Pt species into the interlayer galleries of the restacked $HCa_2Nb_3O_{10}$ nanosheets.[S2]

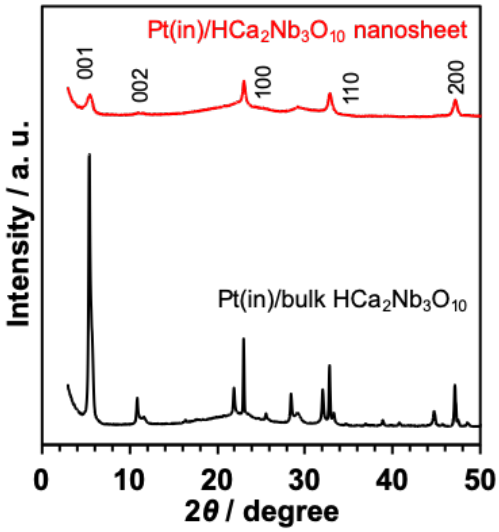

Figure S5. XRD of bulk Pt(in)/$HCa_2Nb_3O_{10}$ and Pt(in)/$HCa_2Nb_3O_{10}$ restacked nanosheets. Sharp diffraction peaks of unexfoliated $HCa_2Nb_3O_{10}$ due to layer staking (for example, 001 and 002) became much broader and less intense after the exfoliation and restacking procedure. However, the (100) and (110) diffraction peaks that arise from in-plane diffraction remained. This result therefore indicates the occurrence of turbostratic ordering of individual sheets in restacked Pt(in)/$HCa_2Nb_3O_{10}$.

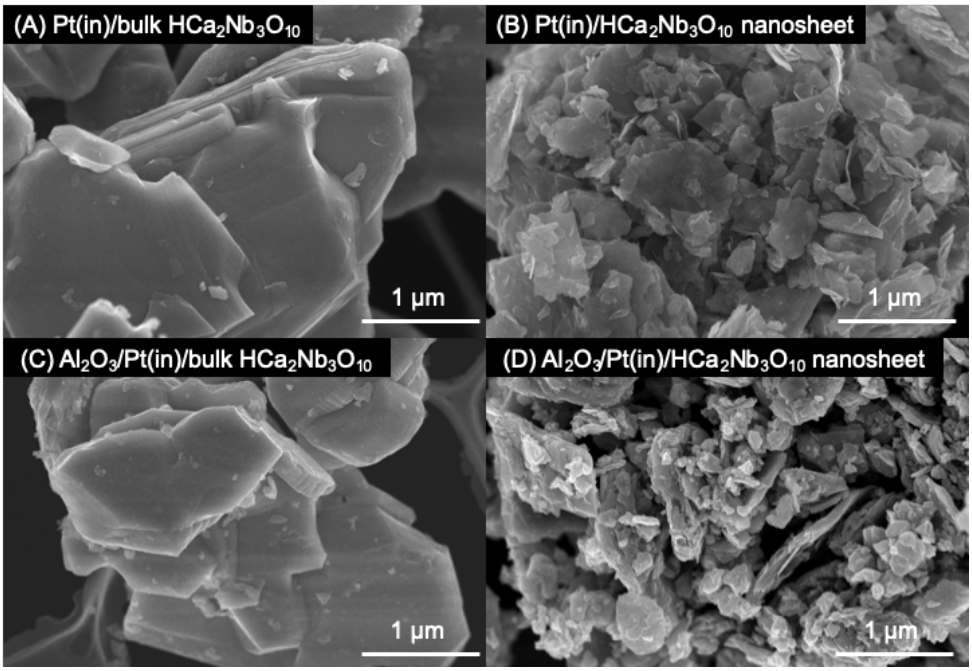

Figure S6. SEM images of (A) bulk Pt(in)/$HCa_2Nb_3O_{10}$ and (B) Pt(in)/$HCa_2Nb_3O_{10}$ restacked nanosheets. Panels (C) and (D) indicate data for Al_2O_3-loaded specimens. The SEM observations show that bulk specimens have a plate-like morphology, while a disordered rough surface structure was seen for the restacked $HCa_2Nb_3O_{10}$ nanosheets. No morphology change was seen after Al_2O_3 deposition on the $HCa_2Nb_3O_{10}$ nanosheets. The specific surface area of the Pt(in)/$HCa_2Nb_3O_{10}$ restacked nanosheets (37 $m^2\ g^{-1}$) was one order of magnitude higher than that of bulk Pt(in)/$HCa_2Nb_3O_{10}$ (2.3 $m^2\ g^{-1}$).

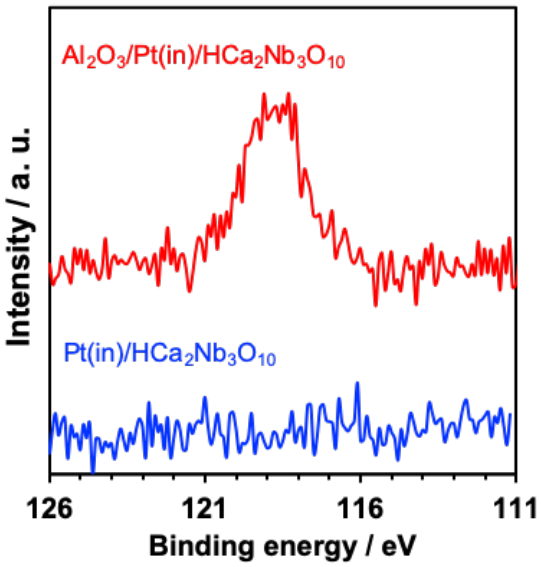

Figure S7. Al-2s XPS spectra of $Pt(in)/HCa_2Nb_3O_{10}$ and $Al_2O_3/Pt(in)/HCa_2Nb_3O_{10}$ nanosheets.

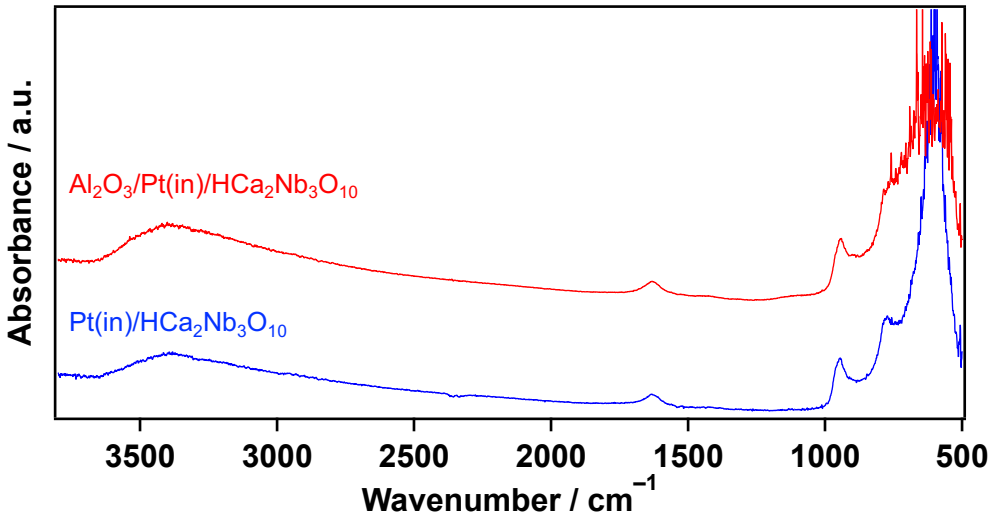

Figure S8. FT-IR spectra of $Pt(in)/HCa_2Nb_3O_{10}$ and $Al_2O_3/Pt(in)/HCa_2Nb_3O_{10}$ nanosheets. The spectral shapes of these specimens are similar to each other, and also identical to those reported in previous studies of restacked $Ca_2Nb_3O_{10}^-$ nanosheets,[S3-4] although the spectra are not very clear in the 800–500 cm^{-1} region. Here, the fact that no peak is seen in the 1200–1000 cm^{-1} region for the $Al_2O_3/Pt(in)/HCa_2Nb_3O_{10}$ nanosheets indicates the absence of AlOOH and $Al(OH)_3$ on the surface of $Pt(in)/HCa_2Nb_3O_{10}$ nanosheets. Previous works have indicated that AlOOH has characteristic absorbance peaks at around 1160 and 1080 cm^{-1}, which are respectively assigned to the symmetric and asymmetric bending vibrations of Al–O–H in the AlOOH lattice.[S5] It has been also reported that $Al(OH)_3$ has absorbance peaks at 970 and 1020 cm^{-1}, which are related to bending modes of OH groups.[S6-7] Peaks attributed to NO_3^- and hydrocarbon species, which respectively appear in the 1400–1300 and 3000–2800 cm^{-1} regions,[S8-10] are also absent, indicating that the amount of residual NO_3^- and/or TBA^+ in these nanosheet materials is negligible.

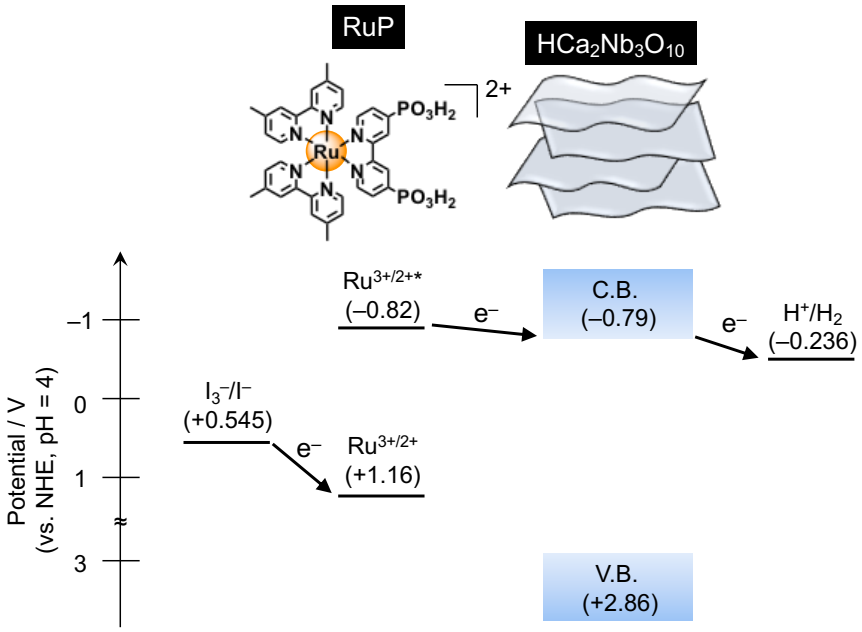

Figure S9. Energy diagram of $HCa_2Nb_3O_{10}$ and **RuP** photosensitizer together with the redox potentials of H^+/H_2 and I_3^-/I^- at pH = 4.

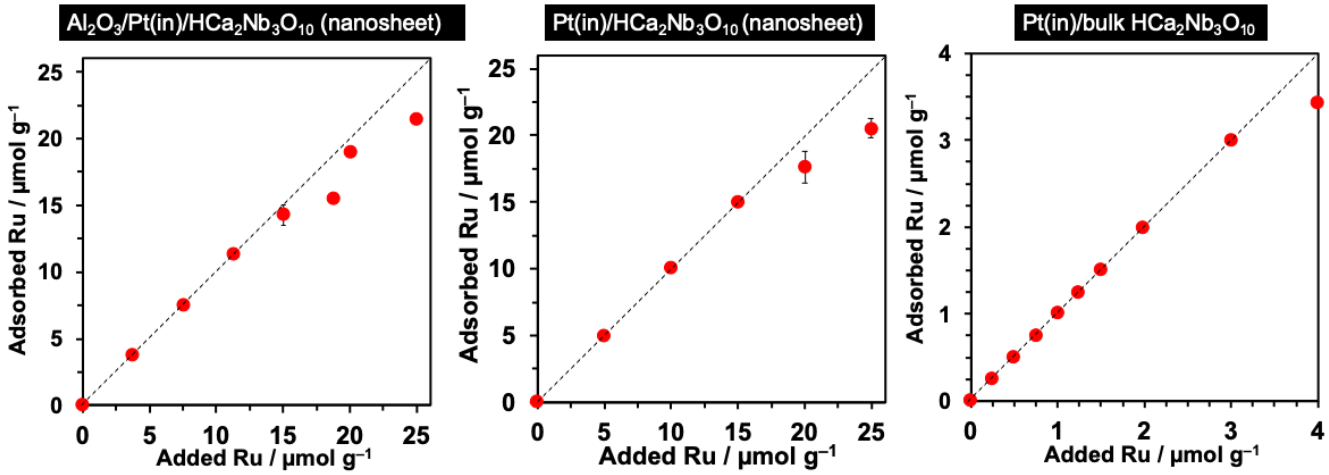

Figure S10. Adsorption isotherms of **RuP** on Al_2O_3/Pt(in)/$HCa_2Nb_3O_{10}$ nanosheets, Pt(in)/$HCa_2Nb_3O_{10}$ nanosheets, and Pt(in)/layered bulk $HCa_2Nb_3O_{10}$ at room temperature.

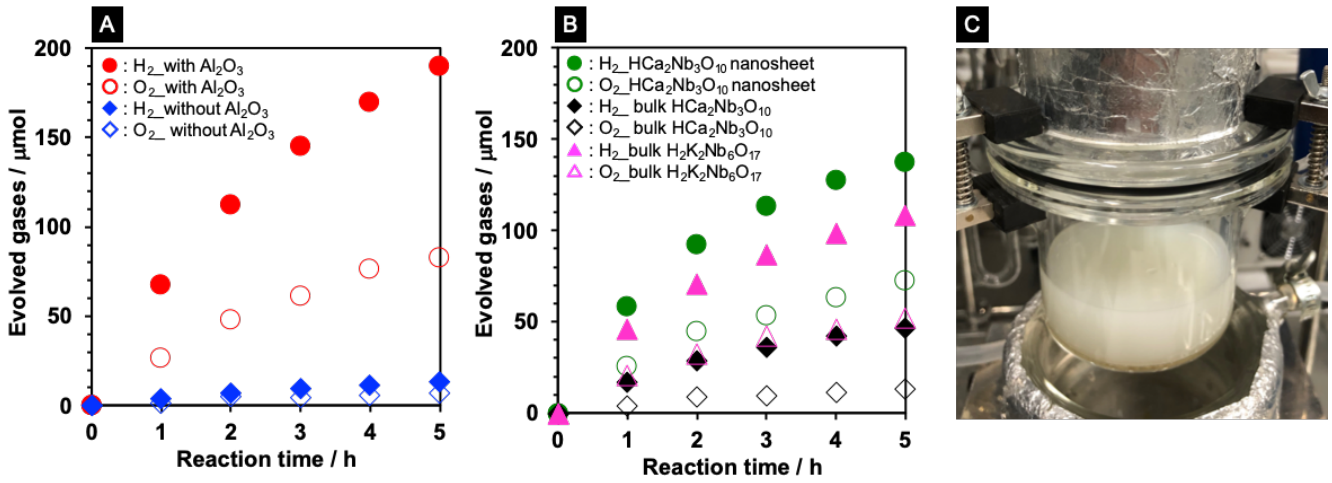

Figure S11. Time courses of Z-scheme water splitting over **RuP**-sensitized nanosheets and layered bulk compounds. H_2 evolution catalyst: (A) **RuP** (15 μmol g^{-1})/Pt(in)/$HCa_2Nb_3O_{10}$ with and without Al_2O_3 deposition and (B) Pt-intercalated $HCa_2Nb_3O_{10}$ nanosheets, bulk $HCa_2Nb_3O_{10}$, and bulk $H_2K_2Nb_6O_{17}$ modified with **RuP** (3 μmol g^{-1}) and Al_2O_3. Reaction conditions: H_2 evolution catalyst, 20 mg; PtO_x/H-Cs-WO_3, 50 mg; solution, 10 mM aqueous NaI solution (pH = 4, 100 mL). The data correspond to those shown in Table 1. The panel (C) indicates a picture of a typical photocatalyst suspension.

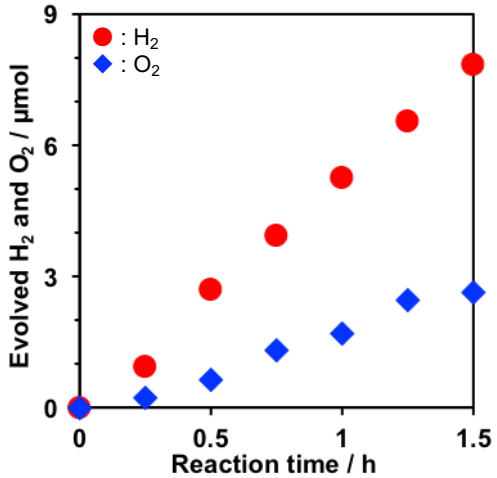

Figure S12. Z-scheme water splitting over **RuP** (10 μmol g^{-1})/Al_2O_3/Pt(in)/$HCa_2Nb_3O_{10}$ nanosheets and PtO_x/H-Cs-WO_3 under simulated sunlight irradiation (AM1.5G, 100 mW cm^{-2}). Reaction conditions: **RuP**/Al_2O_3/Pt(in)/$HCa_2Nb_3O_{10}$, 20 mg; PtO_x/H-Cs-WO_3, 50 mg; solution, 10 mM aqueous NaI solution (pH = 4, 100 mL). Solar-to-hydrogen conversion efficiency (STH) was calculated according to the following equation:

$$\mathrm{STH}\ (\%) = 2 \times R_O \times \Delta G^o / (P \times S) \times 100$$

where R_O, ΔG^o, P and S are the rate of oxygen evolution (mol s^{-1}) in Z-scheme water splitting, the standard Gibbs free energy of water (237×10^3 J mol^{-1}), the intensity of simulated sunlight (100 mW cm^{-2}), and the irradiation area (9 cm^2), respectively. A HAL-320 solar simulator (Asahi Spectra) was employed as the light source.

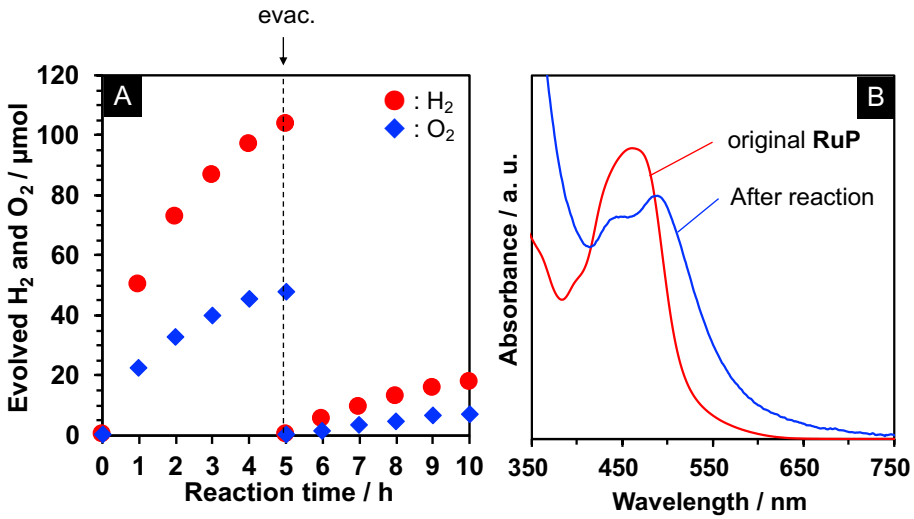

Figure S13. (A) Time course of Z-scheme water splitting over **RuP**(15 μmol g^{-1})/Al_2O_3/Pt(in)/$HCa_2Nb_3O_{10}$ and PtO_x/H–Cs–WO_3. Reaction conditions: **RuP**(15 μmol g^{-1})/Al_2O_3/Pt(in)/$HCa_2Nb_3O_{10}$, 20 mg; PtO_x/H-Cs-WO_3, 50 mg; solution, 10 mM aqueous NaI solution (pH = 4, 100 mL). (B) UV-visible absorption spectrum of the reaction solution after Z-scheme water splitting. The suspended solids were removed by filtration before measurement.

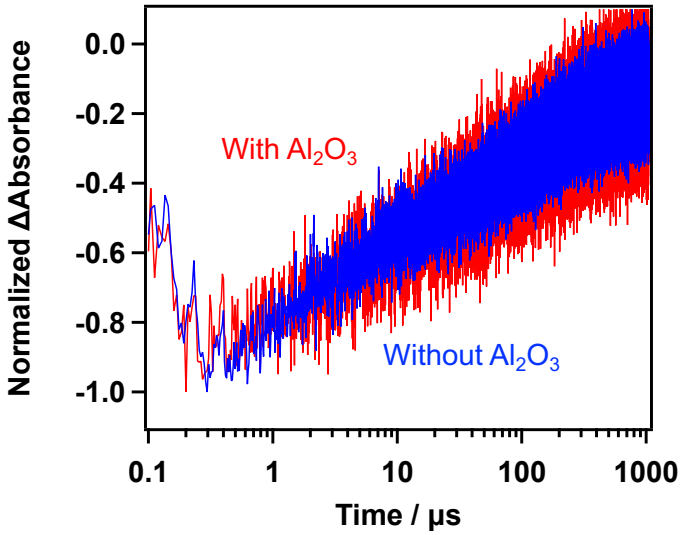

Sample	τ_1 / μs (%)	τ_2 / μs (%)	τ_3 / μs (%)
w Al_2O_3	30 ± 2 (29)	240 ± 20 (40)	3.0 ± 0.3 (31)
w/o Al_2O_3	33 ± 3 (23)	210 ± 10 (38)	2.5 ± 0.1 (39)

Figure S14. Time-dependent absorbance change in transient absorption spectra of **RuP**-sensitized Pt(in)/$HCa_2Nb_3O_{10}$ nanosheets with and without Al_2O_3 modification monitored at 460 nm in H_2O (pH 4). The profiles could be fitted by a triple-exponential function.

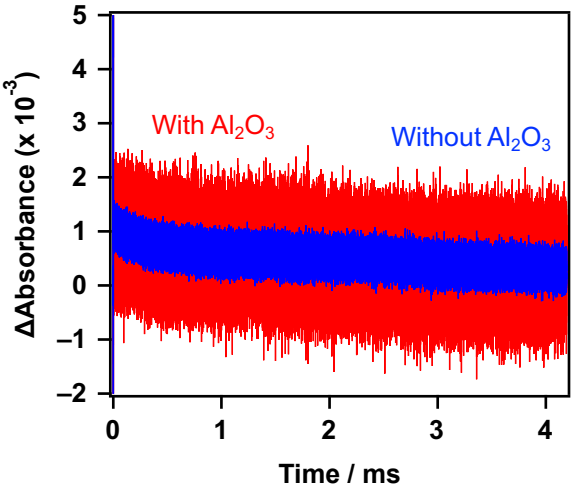

Figure S15. Decay profiles of oxidized I^- species in transient diffuse reflectance spectra of **RuP**-sensitized Pt(in)/$HCa_2Nb_3O_{10}$ nanosheets with and without Al_2O_3 modification recorded at 380 nm in an aqueous NaI solution (0.1 M, pH 3.9).

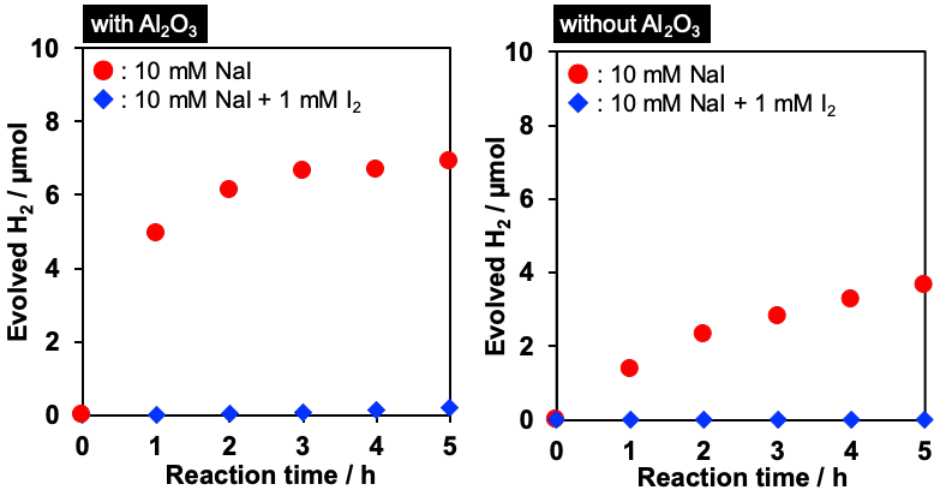

Figure S16. Time courses of H_2 evolution from an aqueous NaI solution over **RuP**(15 μmol g^{-1})/Al_2O_3/Pt(in)/$HCa_2Nb_3O_{10}$ and **RuP**(15 μmol g^{-1})/Pt(in)/$HCa_2Nb_3O_{10}$ in the absence or presence of I_2. Reaction conditions: catalyst, 20 mg; solution, 10 mM aqueous NaI solution (100 mL, pH = 4) or mixed solution of NaI (10 mM) and I_2 (1 mM) (100 mL, pH = 4).

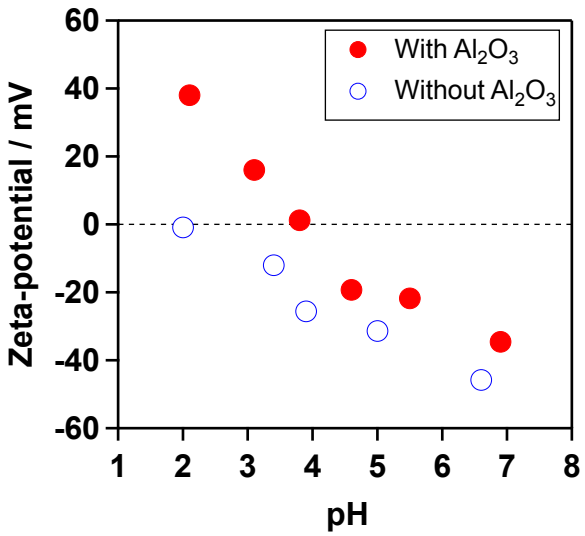

Figure S17. ζ–potentials of Al_2O_3/Pt(in)$HCa_2Nb_3O_{10}$ and Pt(in)/$HCa_2Nb_3O_{10}$ nanosheet as a function of pH.

References

S1. Suzuki, H.; Tomita, O.; Higashi, M.; Abe, R. Design of Nitrogen-Doped Layered Tantalates for Non-Sacrificial and Selective Hydrogen Evolution from Water under Visible Light. *J. Mater. Chem. A* **2016,** *4*, 14444-14452.

S2. Oshima, T.; Lu, D.; Ishitani, O.; Maeda, K. Intercalation of Highly Dispersed Metal Nanoclusters into a Layered Metal Oxide for Photocatalytic Overall Water Splitting. *Angew. Chem. Int. Ed.* **2015,** *54*, 2698-2702.

S3. Han, Y.-S.; Park, I.; Choy, J.-H. Exfoliation of Layered Perovskite, $KCa_2Nb_3O_{10}$, into Colloidal Nanosheets by a Novel Chemical Process. *J. Mater. Chem.* **2001,** *11*, 1277-1282.

S4. Ma, J.; Zhang, Z.; Yang, M.; Wu, Y.; Feng, X.; Liu, L.; Zhang, X.; Tong, Z. Intercalated Methylene Blue between Calcium Niobate Nanosheets by ESD Technique for Electrocatalytic Oxidation of Ascorbic Acid. *Microporous Mesoporous Mater.* **2016,** *221*, 123-127.

S5. Zhang, J.; Wei, S.; Lin, J.; Luo, J.; Liu, S.; Song, H.; Elawad, E.; Ding, X.; Gao, J.; Qi, S.; Tang, C. Template-Free Preparation of Bunches of Aligned Boehmite Nanowires. *J. Phys. Chem. B* **2006,** *110*, 21680-21683.

S6. Balan, E.; Lazzeri, M.; Morin, G.; Mauri, F. First-Principles Study of the OH-Stretching Modes of Gibbsite. *Am. Mineral.* **2006,** *91*, 115-119.

S7. Dubovoy, V.; Stranick, M.; Du-Thumm, L.; Pan, L. Development of Ambient Nanogibbsite Synthesis and Incorporation of the Method to Embed Ultrafine Nano-$Al(OH)_3$ into Channels and Partial Alumination of MCM-41. *Cryst. Growth Des.* **2016,** *16*, 1717-1724.

S8. Ross, M. W.; DeVore, T. C. Desorption of Nitric Acid from Boehmite and Gibbsite. *J. Phys. Chem. A* **2008,** *112*, 6609-6620.

S9. Maeda, K.; Ishimaki, K.; Okazaki, M.; Kanazawa, T.; Lu, D.; Nozawa, S.; Kato, H.; Kakihana, M. Cobalt Oxide Nanoclusters on Rutile Titania as Bifunctional Units for Water Oxidation Catalysis and Visible Light Absorption: Understanding the Structure-Activity Relationship. *ACS Appl. Mater. Interfaces* **2017,** *9*, 6114-6122.

S10. Oshima, T.; Ishitani, O.; Maeda, K. Non-Sacrificial Water Photo-Oxidation Activity of Lamellar Calcium Niobate Induced by Exfoliation. *Adv. Mater. Interfaces* **2014,** *1*, 1400131.